Asian Journal of Control, Vol. 16, No. 3, pp. 669–678, May 2014
Published online 19 December 2013 in Wiley Online Library (wileyonlinelibrary.com) DOI: 10.1002/asjc.826

UNIFIED TRACKING AND REGULATION VISUAL SERVO CONTROL FOR WHEELED MOBILE ROBOTS

W. MacKunis, N. Gans, A. Parikh, and W. E. Dixon

ABSTRACT

The problem of unified tracking and regulation visual servo control is addressed in this paper, for a wheeled mobile robot (WMR) equipped with a single monocular camera system. The desired trajectory or desired fixed position and orientation are defined using a prerecorded image sequence (*i.e.*, a video) or a single image (*i.e.*, a snapshot) of four feature points. Euclidean homographies are developed by exploiting the projective geometric relationships that exist between the feature points in the live image and the prerecorded sequence of images and the corresponding feature points in a fixed reference image. The information obtained from the Euclidean homographies is then utilized to recast the WMR kinematics in a standard WMR form. A rigorous Lyapunov-based analysis is provided to show that the proposed visual servo control approach achieves simultaneous tracking and regulation control for the on-board camera-in-hand problem.

Key Words: Nonlinear control, adaptive control, visual servo control.

I. INTRODUCTION

Wheeled mobile robot (WMR) control researchers have targeted the problems of: stabilization of a robot about a geometric path; stabilization of a robot about a time varying trajectory; and stabilizing the vehicle to a desired set point. Stabilization of the WMR to a desired set point is challenging due to the structure of the governing differential equations. That is, due to the implications of Brockett's condition [1], the set point stabilization control problem cannot be solved via a smooth, time-invariant state feedback law. In light of this obstacle, some researchers have proposed controllers that utilize discontinuous control laws, piecewise continuous control laws, smooth time-varying control laws, or hybrid controllers to achieve set point regulation (see [2], and the references therein for an in-depth review of the previous work). A disturbance observer-based control approach is presented in [3] to achieve tracking control of an omnidirectional mobile robot. The method in [3] utilizes a generalized proportional integral-based observer to compensate for the effects of additive nonlinear input perturbations. In [4], intelligent control methods are proposed to improve tracking performance in nonholonomic mobile robots. The techniques presented in [4] involve replacing the proportional and differential terms in a nonlinear control law with fuzzy functions. In [5], a finite-time tracking control method for nonholonomic mobile robots is presented under the restriction that the desired velocities satisfy a given set of conditions. The result in [5] is achieved by dividing the error dynamics into two subsystems and designing controllers for each of the subsystems. In [6], a transverse function (TF)-based approach is utilized to achieve practical stabilization of arbitrary reference trajectories, including fixed-points and nonadmissible trajectories. The first result that solved the unified tracking and regulation problem with a continuous controller is given in [7]. In [7], a global exponential tracking and regulation result was developed by using an exogenous damped dynamic oscillator. A variety of controllers have since been developed that were inspired by the dynamic oscillator structure in [7] (e.g., see [2,8] and our preliminary work in [9]).

In addition to the above WMR research, which has focused on the control problem assuming that the Euclidean states of the vehicle are known, additional research has focused on the control via different sensor modalities [10]. Of these approaches, advances in computer vision systems have spawned significant efforts focused on vision-based control of mobile vehicles. Image-based visual-servoing (IBVS) is a popular approach to vision-based control. In [11], an image-based visual servo controller was proposed for a mobile manipulator application; however, the result requires geometric distances associated with the object to be known and relies

Manuscript received December 17, 2012; revised August 7, 2013; accepted September 19, 2013.

William MacKunis (corresponding author, e-mail: william.mackunis@erau.edu) is with the Department of Physical Sciences, Embry-Riddle Aeronautical University, Daytona Beach, FL 32114.

Nicholas Gans (e-mail: ngans@utdallas.edu) is with the Department of Electrical Engineering, University of Texas at Dallas, Richardson, TX 75083.

Anup Parikh (e-mail: anuppari@ufl.edu) and Warren Dixon (e-mail: wdixon@ufl.edu) are with the Department of Mechanical and Aerospace Engineering, University of Florida, Gainesville, FL 32611-6250.

This research is supported in part by the AFRL Mathematical Modeling and Optimization Institute. Any opinions, findings, and conclusions or recommendations expressed in this material are those of the authors and do not necessarily reflect the views of the sponsoring agency.

© 2013 Chinese Automatic Control Society and Wiley Publishing Asia Pty Ltd

on an image-Jacobian that contains singularities for some configurations. Moreover, the result in [11] requires the additional degrees-of-freedom from the manipulator to regulate the orientation of the camera. An IBVS method for WMR set-point stabilization is presented in [12] using epipolar geometry. Epipolar geometry-based visual servoing has some inherent drawbacks, however, including baseline degeneracies and the requirement of many feature points. To overcome the drawbacks associated with epipolar geometry, an estimation technique is proposed in [13] to achieve set-point stabilization of a WMR despite lack of depth information. The technique in [13] exploits elements from both image-based and position-based visual servo control methods by incorporating a combination of image signals and a rotation error estimate in the system error vector definition. In [14], a spherical image projection of a monocular vision system is used, which relies on teaching and replay phases to facilitate the estimation of an unknown object height parameter in the image-Jacobian by solving a least-squares problem. In addition to estimation techniques, adaptive control methods can be utilized to compensate for system uncertainty. In [15], Dixon *et al*. used feedback from an uncalibrated, fixed (ceiling-mounted) camera to develop an adaptive tracking controller for a WMR that compensated for the parametric uncertainty in the camera and the WMR dynamics.

Recently, several authors have explored the use of homography-based visual servo control methods for WMRs. The homography-based approach exploits a combination of reconstructed Euclidean information and image-space information in the control design. The Euclidean information is reconstructed by decoupling the interaction between translation and rotation components of a homography matrix. Some potential advantages of this methodology over the aforementioned approaches are that an accurate Euclidean model of the environment (or target image) is not required and potential singularities in the image-Jacobian are eliminated because the image-Jacobian for homography-based visual servo controllers can be expressed in block triangular form, where each block is full-rank. By comparing the feature points of an object from a reference image to feature points of an object in the current image and a prerecorded sequence of images, projective geometric relationships are exploited to enable the reconstruction of the Euclidean coordinates of the target points with respect to the WMR coordinate frame. The first use of homography-based visual servo control of a WMR is given in [16]. In [16] a homography-based approach was used in conjunction with a control structure motivated by [17] to achieve the WMR set point regulation problem where the camera was mounted onboard the vehicle (*i.e.*, camera-in-hand problem). The approach was extended to the fixed camera problem (*i.e.*, camera-to-hand) in [18]. Each of the controllers developed in [16,18] uses an adaptive feedforward term to compensate for an unknown depth constant. In [19], Chen *et al*. also solved the WMR tracking control problem; however, due to restrictions on the desired trajectory, the controller could not be applied to also solve the set point stabilization problem. Benhimane *et al*. use a first order local kinematic model of a WMR in [20] to address a follow-the-leader problem in which the follower is required to follow a path based on a reference image viewed on the lead vehicle. Details are not provided regarding how the authors of [20] compensate for the uncertain depth information. A homography-based visual servo controller is presented in [21], which combines motion planning techniques with methods from hybrid systems to enable a WMR to track optimal paths in Cartesian space. A key factor enabling the control technique in [21] is that the qualitative structure of the optimal paths is known *a priori*. Utilizing the optimal scheme in [22], the control method in [21] achieves tracking in the presence of camera field-of-view (FOV) constraints without estimating the pose parameters.

The contribution of this paper is the development that illustrates how state information determined from the homography decomposition can be used to formulate the WMR kinematic model in a form that is amenable to control designs that solve the unified tracking and regulation WMR visual servo control problem. Specifically, with minimal knowledge of target points on a fixed reference plane, a geometric reconstruction technique is utilized to determine a constant depth parameter, then a series of transformations yields a kinematic model that is developed in terms of signals acquired from the homography decomposition that is in the form of Brockett's nonholonomic integrator. Once the model has been expressed in the form of the nonholonomic integrator, then several of the recently developed class of controllers that solve the unified tracking and regulation problem can be applied. For example, we apply a controller originally developed in [7] to yield a uniformly ultimately bounded (UUB) tracking and regulation result for the camera-in hand problem.

II. GEOMETRIC MODEL

As shown in Fig. 1, the origin of an orthogonal body-fixed coordinate system ${}^{B}\mathcal{F}$ attached to the onboard camera is coincident with the center of mass of the WMR. As also shown in Fig. 1, the x-axis and y-axis of ${}^{B}\mathcal{F}$ define the plane of motion where the x-axis of ${}^{B}\mathcal{F}$ is perpendicular to the wheel axis, and the y-axis is parallel to the wheel axis. The z-axis of ${}^{B}\mathcal{F}$ is perpendicular to the plane of motion and is located at the center of mass of the WMR. The linear velocity of the WMR along the x-axis of ${}^{B}\mathcal{F}$ is denoted by $v_c(t) \in \mathbb{R}$, and the angular velocity $\omega_c(t) \in \mathbb{R}$ is about the z-axis. As shown in Fig. 1, the desired robot trajectory expressed in the

© 2013 Chinese Automatic Control Society and Wiley Publishing Asia Pty Ltd

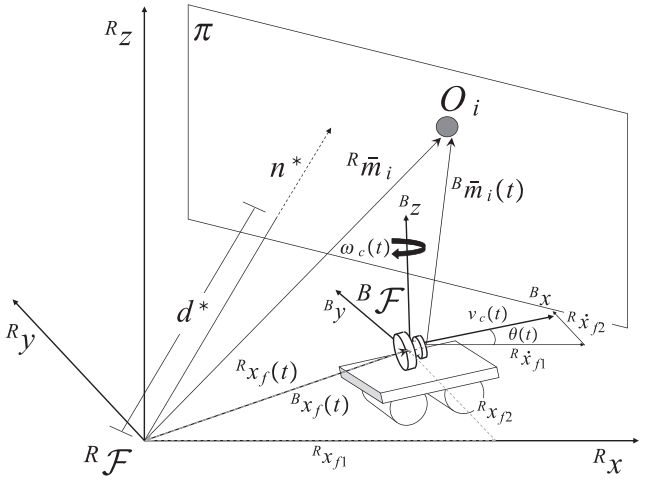

Fig. 1. Geometric relationships between the body-fixed frame $^B\mathcal{F}$ and the fixed reference frame $^R\mathcal{F}$ showing the WMR displacement vectors $^B x_f(t)$ (dashed gray arrow). $^R x_f(t)$ (solid black arrow), desired WMR position vector $^R x_{df}(t)$, and rotational velocity $\omega_c(t)$.

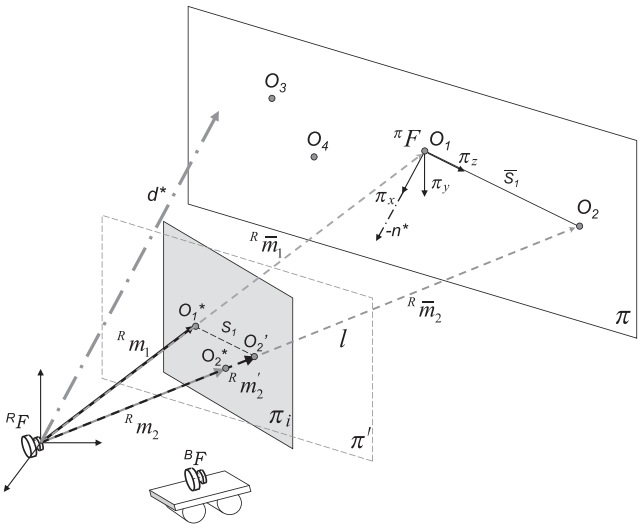

Fig. 2. Diagram illustrating the unknown distance d^*; the camera image plane π_i containing image points O_1^* and O_2^*; the target plane π with target points O_i for $i \in \{1, 2, 3, 4\}$; and the reference frames $^R\mathcal{F}$, $^B\mathcal{F}$, and $^\pi\mathcal{F}$.

desired, time-varying coordinate system $^d\mathcal{F}$ is obtained from a prerecorded set of images of a stationary target viewed and recorded by the onboard camera as the WMR moves. For example, the desired WMR motion could be obtained as an operator drives the robot via a teach pendant, with the onboard camera capturing and storing the sequence of images of the stationary target. A fixed orthogonal coordinate system, denoted by $^R\mathcal{F}$, represents a fixed (single snapshot) reference position and orientation of the camera relative to the stationary target plane $^\pi\mathcal{F}$. For example, the fixed coordinate system $^R\mathcal{F}$ could be the position and orientation at the initial time t_0.

Fig. 2 shows the geometric relationships between the coordinate systems $^B\mathcal{F}$ and $^R\mathcal{F}$, and a reference plane π that contains four target points O_i for $i \in \{1, 2, 3, 4\}$ that are not collinear. It is assumed that the distance $\bar{S}_1$ between the target points O_1 and O_2 is known. The normalized Euclidean coordinates of these image points expressed in $^B\mathcal{F}$ and $^R\mathcal{F}$ are given by $m_i(t)$, $m_{Ri} \in \mathbb{R}^3$, respectively, and the desired image coordinates $m_{di}(t)$ can be expressed in terms of $^d\mathcal{F}$ as

$$m_i(t) = \begin{bmatrix} 1 & m_{iy}(t) & m_{iz}(t) \end{bmatrix}^T = \frac{\bar{m}_i(t)}{x_i(t)}$$
$$m_{di}(t) = \begin{bmatrix} 1 & m_{diy}(t) & m_{diz}(t) \end{bmatrix}^T = \frac{\bar{m}_{di}(t)}{x_{di}(t)} \quad (1)$$
$$m_{Ri} = \begin{bmatrix} 1 & m_{iy} & m_{iz} \end{bmatrix}^T = \frac{\bar{m}_{Ri}}{x_{Ri}}$$

under the standard assumption that the distances from the origin of the respective coordinate frames to the targets along the focal axis remains positive (*i.e.*, $x_i(t)$, $x_{di}(t)$, $x_{Ri} \geq \varepsilon > 0$ where ε is an arbitrarily small positive constant). In (1), $\bar{m}_i(t)$, $\bar{m}_{di}(t)$, $\bar{m}_{Ri} \in \mathbb{R}^3$ denote the (unnormalized) Euclidean coordinates of the target points O_i. As shown in Fig. 2, a projection of the target points O_i is captured by the WMR camera, resulting in a set of image points O_i^* for $i \in \{1, 2, 3, 4\}$ in the image plane π_i. The image points O_i^* will have projected pixel coordinates, which are denoted by $u_{Bi}(t)$, $v_{Bi}(t) \in \mathbb{R}$ for $^B\mathcal{F}$, $u_{di}(t)$ $v_{di}(t) \in \mathbb{R}$ for $^d\mathcal{F}$, and u_{Ri}, $v_{Ri} \in \mathbb{R}$ for $^R\mathcal{F}$. The pixel coordinates $u_{Bi}(t)$, $v_{Bi}(t)$; $u_{di}(t)$, $v_{di}(t)$; and u_{Ri}, v_{Ri} are defined as elements of $p_{Bi}(t) \in \mathbb{R}^3$ (*i.e.*, the time-varying image points), $p_{di}(t) \in \mathbb{R}^3$ (*i.e.*, the desired image point trajectory), and $p_{Ri} \in \mathbb{R}^3$ (*i.e.*, the constant reference image points), respectively, as

$$p_{Bi} = \begin{bmatrix} 1 & v_{Bi} & u_{Bi} \end{bmatrix}^T \quad p_{di} = \begin{bmatrix} 1 & v_{di} & u_{di} \end{bmatrix}^T$$
$$p_{Ri} = \begin{bmatrix} 1 & v_{Ri} & u_{Ri} \end{bmatrix}^T. \quad (2)$$

The normalized Euclidean coordinates of the target points are related to the image data via the pinhole lens models

$$p_{Bi} = Am_i \quad p_{di} = Am_{di} \quad p_{Ri} = Am_{Ri}, \quad (3)$$

where $A \in \mathbb{R}^{3\times3}$ is a known, constant, intrinsic camera calibration matrix.

The rotation from $^R\mathcal{F}$ to $^B\mathcal{F}$ is denoted by $R_B(\theta) \in SO(3)$, and the desired time-varying rotation from $^R\mathcal{F}$ to $^d\mathcal{F}$ is denoted by $R_D(\theta_d) \in SO(3)$, where $\theta(t) \in \mathbb{R}$ denotes the right-handed rotation angle about $z_i(t)$ that aligns the orientation of $^B\mathcal{F}$ with $^R\mathcal{F}$ and $\theta_d(t) \in \mathbb{R}$ denotes the right-handed rotation angle about $z_{di}(t)$ that aligns the desired orientation of $^d\mathcal{F}$ with $^R\mathcal{F}$. The translation from $^B\mathcal{F}$ to $^R\mathcal{F}$ is denoted by $x_f(t) \in \mathbb{R}^3$, where $x_f(t)$ is expressed in $^B\mathcal{F}$, and the desired translation from $^d\mathcal{F}$ to $^R\mathcal{F}$ is denoted by

© 2013 Chinese Automatic Control Society and Wiley Publishing Asia Pty Ltd

$x_{df}(t) \in \mathbb{R}^3$, where $x_{df}(t)$ is expressed in ${}^{d}\mathcal{F}$. Since the motion of the WMR is constrained to the xy-plane, $x_f(t)$ and $x_{df}(t)$ are defined as

$$x_f(t) \triangleq \begin{bmatrix} x_{f1}(t) & x_{f2}(t) & 0 \end{bmatrix}^T \tag{4}$$

$$x_{df}(t) \triangleq \begin{bmatrix} x_{df1}(t) & x_{df2}(t) & 0 \end{bmatrix}^T. \tag{5}$$

The following coordinate transformations can be determined [16,18]:

$$\bar{m}_i = R_B \bar{m}_{Ri} + x_f, \quad \bar{m}_{di} = R_D \bar{m}_{Ri} + x_{df}. \tag{6}$$

The angular velocities can be expressed as $\omega_c = -\dot{\theta}$ and $\omega_{cd} = -\dot{\theta}_d$, where $\omega_{cd}(t) \in \mathbb{R}$ denotes the desired angular velocity of the WMR expressed in ${}^{d}\mathcal{F}$. The rotation angles are assumed to satisfy the inequalities $-\frac{\pi}{2} \le \theta(t) \le \frac{\pi}{2}$ and $-\frac{\pi}{2} \le \theta_d(t) \le \frac{\pi}{2}$. (Although it is assumed that the target points never leave the FOV of the camera, recent Daisy-chaining results show how target points out of the FOV can be related to image points in the FOV [23].) The plane π has normal vector $-n^*$ as expressed in ${}^{R}\mathcal{F}$. The distance $d^* \in \mathbb{R}^+$ from ${}^{R}\mathcal{F}$ to π along the unit normal n^* of π is given by

$$d^* = (n^*)^T \bar{m}_{Ri}. \tag{7}$$

Using (7), the expressions given in (6) can be rewritten as

$$\bar{m}_i = H \bar{m}_{Ri}, \quad \bar{m}_{di} = H_d \bar{m}_{Ri}, \tag{8}$$

respectively, where $H(t)$, $H_d(t) \in \mathbb{R}^{3\times 3}$ are Euclidean homographies. By using (4) along with the definitions of the rotation matrices $R_B(t)$ and $R_D(t)$, $H(t)$ can be expressed as

$$H = \begin{bmatrix} \cos\theta + \frac{x_{f1} n_x^*}{d^*} & -\sin\theta + \frac{x_{f1} n_y^*}{d^*} & \frac{x_{f1} n_z^*}{d^*} \\ \sin\theta + \frac{x_{f2} n_x^*}{d^*} & \cos\theta + \frac{x_{f2} n_y^*}{d^*} & \frac{x_{f2} n_z^*}{d^*} \\ 0 & 0 & 1 \end{bmatrix} \tag{9}$$

where $n^* = \begin{bmatrix} n_x^* & n_y^* & n_z^* \end{bmatrix}^T$. By examining the terms in (9), it is clear that $H(t)$ contains signals that are not directly obtained from the vision system. That is, $\theta(t)$, $x_f(t)$, and d^* are not directly available from the camera image. The d^* parameter can be determined from knowledge of the distance $\bar{S}_1$. The procedure for determining d^* will be explained in detail in the next section. The six unknown elements of $H_{jk}(t)$ for $j = 1, 2$ and $k = 1, 2, 3$ can be determined indirectly from the image coordinates by solving a set of linear equations. Specifically, by using the definitions given in (1), the expressions given in (8) can be rewritten as

$$m_i = \frac{x_{Ri}}{x_i} H m_{Ri} \quad m_{di} = \frac{x_{Ri}}{x_{di}} H_d m_{Ri}, \tag{10}$$

respectively, where $\frac{x_{Ri}}{x_i} = \gamma_i(t) \in \mathbb{R}$ and $\frac{x_{Ri}}{x_{di}} = \gamma_{di}(t) \in \mathbb{R}$ denote depth ratios. By using (3), the first Euclidean relationship in (10) can be represented as

$$p_{Bi} = \gamma_i A H A^{-1} p_{Ri} \tag{11}$$

$$= \gamma_i G p_{Ri}. \tag{12}$$

Thus, since A is known and $i \in \{1, 2, 3, 4\}$, it is possible to solve a set of linear equations for $G(t)$ to recover $H(t)$, $R_B(t)$, $\frac{x_f(t)}{d^*}$, n^*, and $\gamma_i(t)$. Similarly, for the same four target points in ${}^{d}\mathcal{F}$ and ${}^{R}\mathcal{F}$, the corresponding unknown elements of $H_d(t)$ can be determined. To compute $\theta(t)$ from $R_B(t)$, the following expression can be utilized [18]:

$$\theta = \arccos\left(\frac{1}{2}(tr(R_B) - 1)\right)$$

where $-\frac{\pi}{2} \le \theta(t) \le \frac{\pi}{2}$.

2.1 Calculation of the distance d* from the object plane to the camera frame

From (7), the distance d^* can be determined based on knowledge of the vectors n^* and $\bar{m}_{Ri}$. The development in this section will describe how n^* and $\bar{m}_{Ri}$ and hence, the distance d^*, can be determined based on knowledge of the distance $\bar{S}_1$ between any two target points O_i on the reference plane.

2.1.1 Solving for the distance d*

By utilizing the properties of similar triangles along with knowledge of the distance $\bar{S}_1$ between points O_1 and O_2, the vector magnitudes $\|\bar{m}_{R1}\|$ and $\|\bar{m}_{R2}\|$ can be determined and used to calculate $\bar{m}_{R1}$ and $\bar{m}_{R2}$ as

$$\bar{m}_{R1} = \frac{\|\bar{m}_{R1}\|}{\|m_{R1}\|} m_{R1}, \quad \bar{m}_{R2} = \frac{\|\bar{m}_{R2}\|}{\|m_{R2}\|} m_{R2}. \tag{13}$$

Since n^* can be calculated from the sets of linear algebraic equations in (8) or (11), the distance d^* can be calculated from (7) using the value of $\bar{m}_{R1}$ obtained from (13). The distance d^* is measured in the direction of the normal vector n^* from the origin of ${}^{R}\mathcal{F}$ to the plane π. Similarly, performing these steps using the normal vector $n = R_B(t)n^*$ instead of n^* gives the distance d from the origin of the current WMR camera frame ${}^{B}\mathcal{F}$ to the plane π at any time. Hence, the distance d^* is known, and the Euclidean Homography given in (9) is expressed in terms of known parameters (*i.e.*, $\frac{x_f(t)}{d^*}$ is

© 2013 Chinese Automatic Control Society and Wiley Publishing Asia Pty Ltd

known). The full procedure for this geometric reconstruction technique has been summarized here for brevity (see [9] for complete details).

III. TRANSFORMATION TO NONHOLONOMIC INTEGRATOR

The kinematic equations for the WMR can be determined by taking the time derivative of the Euclidean position as

$$\dot{x}_f = -v_B + x_f \times \omega \tag{14}$$

where $v_B(t)$, $\omega(t) \in \mathbb{R}^3$ denote the linear and angular velocity of the mobile robot expressed in ${}^B\mathcal{F}$ as

$$\begin{aligned} v_B &\triangleq \begin{bmatrix} v_c & 0 & 0 \end{bmatrix}^T \\ \omega &\triangleq \begin{bmatrix} 0 & 0 & \omega_c \end{bmatrix}^T = \begin{bmatrix} 0 & 0 & -\dot{\theta}(t) \end{bmatrix}^T \end{aligned} \tag{15}$$

respectively, where $v_c(t)$, $\omega_c(t) \in \mathbb{R}$ denote the linear and angular velocity of the center of mass of the WMR. The following expressions can be obtained from (14) and (15):

$$\dot{x}_{f1} = -v_c + x_{f2}\omega_c \tag{16}$$

$$\dot{x}_{f2} = -x_{f1}\omega_c. \tag{17}$$

The Euclidean coordinates of the current WMR position and orientation and desired position and orientation can be expressed in the fixed reference frame ${}^R\mathcal{F}$ as $x_{Rf}(t)$, $\theta(t)$, and $x_{Rd}(t)$, $\theta_d(t)$, respectively, where the coordinate transform from ${}^B\mathcal{F}$ to ${}^R\mathcal{F}$ is given by:

$$x_f = -R_B x_{Rf}. \tag{18}$$

After taking the time derivative of (18), the expressions in (16) and (17) can be rewritten in terms of the fixed reference frame as follows:

$$-\dot{x}_{Rf1}\cos\theta + \dot{x}_{Rf2}\sin\theta = -v_c \tag{19}$$

$$-\dot{x}_{Rf1}\sin\theta - \dot{x}_{Rf2}\cos\theta = 0 \tag{20}$$

where (15) was utilized. The system of equations in (19) and (20) can be utilized to obtain the kinematic expressions

$$\dot{x}_{Rf1} = v_c\cos\theta \tag{21}$$

$$\dot{x}_{Rf2} = -v_c\sin\theta. \tag{22}$$

Based on (15), (21), and (22), the WMR kinematics can now be expressed as

$$\dot{q} = S(q)v \tag{23}$$

where $q(t), \dot{q}(t) \in \mathbb{R}^3$ are defined as

$$q = \begin{bmatrix} x_{Rf1} & x_{Rf2} & \theta \end{bmatrix}^T \quad \dot{q} = \begin{bmatrix} \dot{x}_{Rf1} & \dot{x}_{Rf2} & \dot{\theta} \end{bmatrix}^T, \tag{24}$$

the matrix $S(q) \in \mathbb{R}^{3\times 2}$ is defined as

$$S(q) = \begin{bmatrix} \cos(\theta) & 0 \\ -\sin(\theta) & 0 \\ 0 & 1 \end{bmatrix}, \tag{25}$$

and the velocity vector is defined as

$$v(t) \triangleq \begin{bmatrix} v_1 & v_2 \end{bmatrix}^T = \begin{bmatrix} -v_c & \dot{\theta} \end{bmatrix}^T. \tag{26}$$

Based on the previous development, the kinematic model for the desired trajectory can be expressed as

$$\dot{q}_d = S(q_d)v_d \tag{27}$$

where $q_d(t), \dot{q}_d(t) \in \mathbb{R}^3$ are defined as

$$q_d = \begin{bmatrix} x_{Rd1} & x_{Rd2} & \theta \end{bmatrix}^T \tag{28}$$

$$\dot{q}_d = \begin{bmatrix} \dot{x}_{Rd1} & \dot{x}_{Rd2} & \dot{\theta}_d \end{bmatrix}^T,$$

$S(\cdot)$ was defined in (25), $v_d(t) \triangleq \begin{bmatrix} v_{1d} & v_{2d} \end{bmatrix}^T \in \mathbb{R}^2$ denotes the desired time-varying linear and angular velocity, and $x_{Rd1}(t)$, $x_{Rd2}(t) \in \mathbb{R}$ denote the desired linear velocity components as expressed in ${}^R\mathcal{F}$. With regard to (27), it is assumed that the signal $v_d(t)$ is constructed to produce the desired motion and that $v_d(t)$, $\dot{v}_d(t)$, $q_d(t)$, and $\dot{q}_d(t)$ are bounded for all time.

IV. MODEL TRANSFORMATION

The control objective is to force the WMR to follow a desired time-varying trajectory or move to a desired fixed position and orientation by following a sequence of prerecorded camera images or a single image of the stationary reference points O_i. To quantify the control objective, let $\tilde{x}_{f1}(t)$, $\tilde{x}_{f2}(t)$, $\tilde{\theta}(t) \in \mathbb{R}$ be the difference between the actual WMR position and orientation and the desired position and orientation as

$$\begin{aligned} \tilde{x}_{f1} = x_{Rf1} - x_{Rd1} \quad \tilde{x}_{f2} = x_{Rf2} - x_{Rd2} \\ \tilde{\theta} = \theta - \theta_d \end{aligned} \tag{29}$$

where $x_{Rf1}(t)$, $x_{Rf2}(t)$, $\theta(t)$ are defined in (24), and $x_{Rd1}(t)$, $x_{Rd2}(t)$, $\theta_d(t) \in \mathbb{R}$ represent the desired WMR position and orientation.

To rewrite the kinematic model given in (23) in a form that facilitates the subsequent unified tracking and regulation control synthesis and stability analysis, a global invertible transformation is defined as [7]

© 2013 Chinese Automatic Control Society and Wiley Publishing Asia Pty Ltd

$$\begin{bmatrix} w \\ z_1 \\ z_2 \end{bmatrix} = \Omega \begin{bmatrix} \tilde{x}_{f1} \\ \tilde{x}_{f2} \\ \tilde{\theta} \end{bmatrix} \tag{30}$$

where $\Omega(t) \in \mathbb{R}^{3\times3}$ is defined as

$$\Omega = \begin{bmatrix} -\tilde{\theta}\cos\theta + 2\sin\theta & \tilde{\theta}\sin\theta + 2\cos\theta & 0 \\ 0 & 0 & 1 \\ \cos\theta & -\sin\theta & 0 \end{bmatrix} \tag{31}$$

$w(t) \in \mathbb{R}$ and $z(t) = [z_1(t)\ z_2(t)]^T \in \mathbb{R}^2$ are auxiliary tracking error variables, and $\tilde{x}_{f1}(t)$, $\tilde{x}_{f2}(t)$, $\tilde{\theta}(t)$ were defined in (29).

After taking the time derivative of (30) and using (23), we can rewrite the tracking error dynamics in a form that is similar to Brockett's nonholonomic integrator [1,7] as follows:

$$\dot{w} = u^T J^T z + f \tag{32}$$

$$\dot{z} = u$$

where $J \in \mathbb{R}^{2\times2}$ is a constant, skew symmetric matrix defined as

$$J = \begin{bmatrix} 0 & -1 \\ 1 & 0 \end{bmatrix} \tag{33}$$

and $f(z, v_d, t) \in \mathbb{R}$ is an auxiliary signal defined as

$$f = 2(v_{2d} z_2 - v_{1d} \sin z_1). \tag{34}$$

In (32), the auxiliary kinematic control input $u(t) = [u_1(t)\ u_2(t)]^T \in \mathbb{R}^2$ is defined in terms of the position and orientation, the linear and angular velocities, and the reference (desired) trajectory as follows:

$$u = T^{-1} v + \begin{bmatrix} v_{2d} \\ v_{1d}\cos\tilde{\theta} \end{bmatrix}$$

$$v = Tu + \begin{bmatrix} v_{1d}\cos\tilde{\theta} + v_{2d}(\tilde{x}_{f1}\sin\theta + \tilde{x}_{f2}\cos\theta) \\ v_{2d} \end{bmatrix} \tag{35}$$

where the globally invertible matrix $T(t) \in \mathbb{R}^{2\times2}$ is defined as

$$T = \begin{bmatrix} (\tilde{x}_{f1}\sin\theta + \tilde{x}_{f2}\cos\theta) & 1 \\ 1 & 0 \end{bmatrix}. \tag{36}$$

Remark 1. Based on the fact that $\Omega(t)$ in (31) can be inverted as

$$\Omega^{-1} = \begin{bmatrix} \frac{1}{2}\sin\theta & 0 & \frac{1}{2}\left(\tilde{\theta}\sin\theta + 2\cos\theta\right) \\ \frac{1}{2}\cos\theta & 0 & -\frac{1}{2}\left(\tilde{\theta}\cos\theta - 2\sin\theta\right) \\ 0 & 1 & 0 \end{bmatrix} \tag{37}$$

it is clear from (30) that if $w(t)$, $z_1(t)$, $z_2(t) \in \mathcal{L}_\infty$ then $\tilde{x}_{f1}(t)$, $\tilde{x}_{f2}(t)$, $\tilde{\theta}(t) \in \mathcal{L}_\infty$. Moreover, we can conclude that if $w(t)$, $z_1(t)$, and $z_2(t)$ approach zero as $t \to \infty$, then $\tilde{x}_{f1}(t)$, $\tilde{x}_{f2}(t)$, and $\tilde{\theta}(t)$ approach zero as $t \to \infty$. If $\tilde{\theta}(t)$ approaches zero as $t \to \infty$, then the difference between $R_B(\theta)$ and $R_D(\theta_d)$ becomes the identity. Based on these facts, (6) and (29) can be used to conclude that the Euclidean coordinates $\bar{m}_i(t)$ and $\bar{m}_{di}(t)$ asymptotically align.

V. CONTROL DEVELOPMENT

Now that the WMR kinematics and tracking error dynamics are in the standard forms given in (23) and (32), respectively, many controllers could be used to achieve the simultaneous tracking and regulation control objective. For completeness, we present the controller developed in [7] as an example. To this end, we define an auxiliary error signal $\tilde{z}(t) \in \mathbb{R}^2$ as the difference between the subsequently designed auxiliary signal $z_d(t) \in \mathbb{R}^2$ and the transformed variable $z(t)$, defined in (30), as follows

$$\tilde{z} = z_d - z. \tag{38}$$

Based on the dynamic equations given in (32) and the subsequent stability analysis, the auxiliary signal $u(t)$ is designed as [7]

$$u = u_a - kz \tag{39}$$

where $k \in \mathbb{R}$ is a positive, constant control gain, the auxiliary control term $u_a(t) \in \mathbb{R}^2$ is defined as

$$u_a = \left(\frac{kw + f}{\delta_d^2}\right) J z_d + \Omega_1 z_d. \tag{40}$$

The auxiliary signal $z_d(t) \in \mathbb{R}^2$ is defined by the following oscillator-like relationship [7]:

$$\dot{z}_d = \frac{\dot{\delta}_d}{\delta_d} z_d + \left(\frac{kw + f}{\delta_d^2} + w\Omega_1\right) J z_d \quad z_d^T(0) z_d(0) = \delta_d^2(0) \tag{41}$$

where the auxiliary terms $\Omega_1(t) \in \mathbb{R}$ and $\delta_d(t) \in \mathbb{R}$ are defined as

$$\Omega_1 = k + \frac{\dot{\delta}_d}{\delta_d} + \left(\frac{kw^2 + wf}{\delta_d^2}\right) \tag{42}$$

and

© 2013 Chinese Automatic Control Society and Wiley Publishing Asia Pty Ltd

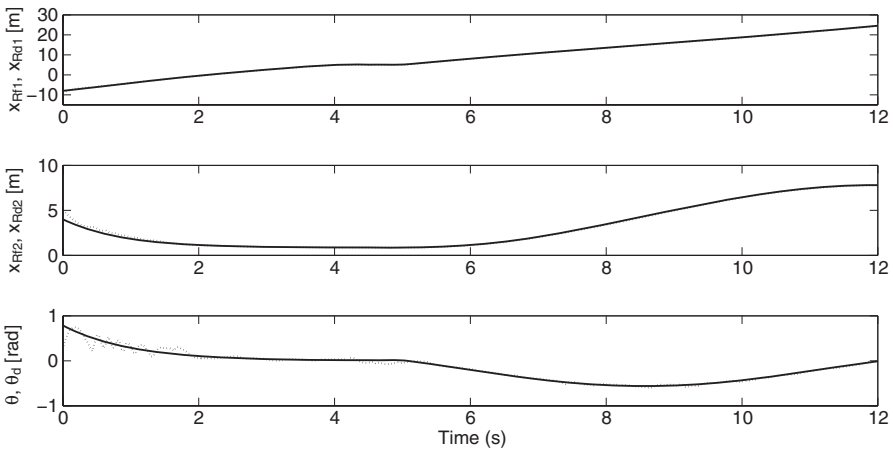

Fig. 3. Desired (solid line) and actual (dotted line) WMR translational position and heading during closed-loop controller operation.

$$\delta_d = \alpha_0 \exp(-\alpha_1 t) + \varepsilon_1 \tag{43}$$

respectively, α_0, α_1, $\varepsilon_1 \in \mathbb{R}$ are positive constant parameters, and $f(z, v_d, t)$ was defined in (34). As described in [7], the closed-loop error dynamics for $w(t)$ can be expressed as

$$\dot{w} = -kw + u_a^T J\tilde{z} \tag{44}$$

and the closed-loop error system for $\tilde{z}(t)$ can be determined as

$$\dot{\tilde{z}} = -k\tilde{z} + wJu_a. \tag{45}$$

VI. STABILITY ANALYSIS

Theorem 1. Given the closed-loop system of (44) and (45), the position/orientation tracking errors defined in (29) are UUB in the sense that

$$|\tilde{x}_{f1}(t)|, |\tilde{x}_{f2}(t)|, |\tilde{\theta}(t)| \le \beta_0 \exp(-\gamma_0 t) + \beta_1 \exp(-\gamma_1 t) + \beta_2 \varepsilon_1 \tag{46}$$

for some positive scalar constants β_0, β_1, β_2, γ_0, and γ_1. Note that ε_1 was originally defined in (43).

Proof. Let $V(t) \in \mathbb{R}$ denote a radially unbounded nonnegative function defined as

$$V(t) = \frac{1}{2}w^2 + \frac{1}{2}\tilde{z}^T\tilde{z}. \tag{47}$$

After taking the time derivative of (47) and making the appropriate substitutions from (44) and (45), the following expression can be obtained

$$\dot{V} \le -2kV. \tag{48}$$

Standard arguments can now be employed to conclude that

$$\|\Psi\| \le \exp(-kt)\|\Psi(0)\| \tag{49}$$

where the vector $\Psi(t) \in \mathbb{R}^3$ is defined as

$$\Psi = \begin{bmatrix} w & \tilde{z}^T \end{bmatrix}^T. \tag{50}$$

Based on (49) and (50), it is straightforward to see that $w(t)$, $\tilde{z}(t) \in \mathcal{L}_\infty$. Based on the fact that $\tilde{z}(t)$, $\delta_d(t) \in \mathcal{L}_\infty$, we can conclude that $z(t)$, $z_d(t) \in \mathcal{L}_\infty$. From (32), (40)–(43), we can show that $u_a(t)$, $\dot{z}_d(t)$, $\Omega_1(t)$, $u(t) \in \mathcal{L}_\infty$. Since $z(t) \in \mathcal{L}_\infty$, it is clear from (29)–(31) that $\tilde{\theta}(t)$, $\theta(t) \in \mathcal{L}_\infty$, and (35) can be used to prove that $v(t) \in \mathcal{L}_\infty$; therefore, it follows from (23)–(26) that $\dot{\theta}(t)$, $\dot{x}_{f1}(t)$, $\dot{x}_{f2}(t) \in \mathcal{L}_\infty$. We can now employ standard signal chasing arguments to conclude that all of the remaining signals in the control and the system remain bounded during closed-loop operation.

To prove the result in (46), the triangle inequality can be applied to (38) to obtain the following exponential bound

$$\|z\| \le \|\tilde{z}\| + \|z_d\| \le \exp(-kt)\|\Psi(0)\| + \alpha_0 \exp(-\alpha_1 t) + \varepsilon_1 \tag{51}$$

where (43) and (49) have been utilized. The main result given by (46) can now be directly obtained from (49)–(51).

Remark 2. We have not imposed any restrictions on the desired trajectory (other than the assumption that $v_d(t)$, $\dot{v}_d(t)$, $q_d(t)$, and $\dot{q}_d(t) \in \mathcal{L}_\infty$); hence, the position and orientation tracking problem reduces to the position and orientation regulation problem. That is, if the control objective is targeted at the regulation problem, the desired position and orientation vector, denoted by $q_d(t) = [x_{df1}(t), x_{df2}(t), \theta_d(t)]^T \in \mathbb{R}^3$ and originally defined in (29), becomes an arbitrary desired constant vector. Based on the fact that q_d is now defined as a constant vector, it is straightforward that $v_d(t)$ given in (27), and consequently $f(z, v_d, t)$ defined in (34), equals zero. We

© 2013 Chinese Automatic Control Society and Wiley Publishing Asia Pty Ltd

also note that the auxiliary variable $u(t)$ originally defined in (35) is now defined as follows

$$u = T^{-1}v \quad v = Tu \tag{52}$$

where the matrix $T(t)$ was defined in (36). Based on the above simplifications, it is easy to show that the result given in (46) is valid for the regulation problem as well.

VII. SIMULATION RESULTS

A numerical simulation was created to verify the performance of the proposed WMR regulation and tracking control law. To develop a realistic stepping stone to experimental validation of the proposed control law, zero-mean Gaussian random noise with a variance of approximately 1 pixel was included in the simulation. Fig. 3 shows the actual and desired position and orientation during closed-loop controller operation. The simulation results in Fig. 3 show the capability of the control law to simultaneously achieve tracking and regulation control. The desired trajectory was designed with a complete stop in the motion of all three states between 4 and 5 seconds. Thus, the WMR is capable of following a time-varying trajectory or regulating to a desired set point using the proposed control law. Fig. 4 shows the position and heading tracking errors, and Fig. 5 shows the control commnds used during closed-loop operation. The control commands remain within reasonable limits throughout the duration of the simulation.

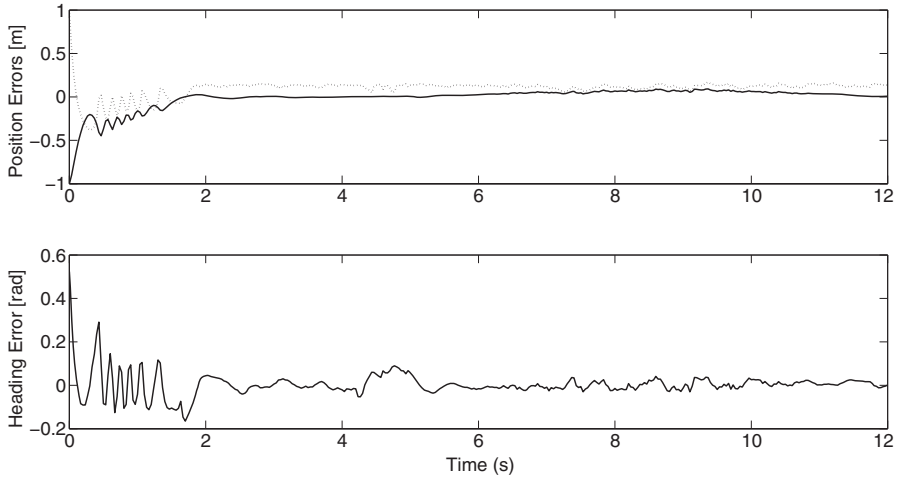

Fig. 4. Position tracking errors (top) and heading error (bottom) during closed-loop operation.

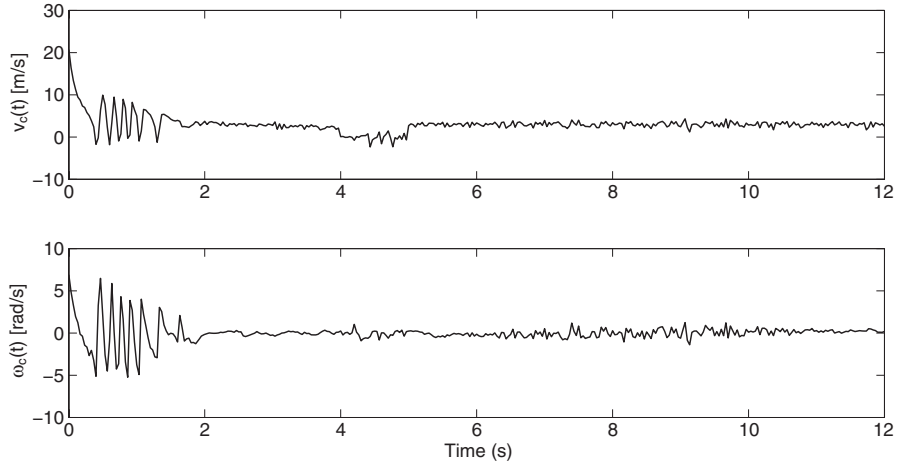

Fig. 5. Commanded forward velocity (top) and angular velocity (bottom) used during closed-loop controller operation.

© 2013 Chinese Automatic Control Society and Wiley Publishing Asia Pty Ltd

VIII. CONCLUSION

A unified tracking and regulation WMR visual servo control result is presented. To yield the result, image geometry is used to relate a desired image (or video sequence) to a reference image so that relative translation and rotation information can be obtained from homography decomposition. Once the depth parameter d^* is calculated using a geometric reconstruction technique, a series of transformations yields a kinematic model that is developed in terms of signals acquired from the homography decomposition that is in the form of Brockett's nonholonomic integrator. Once the model has been expressed in the form of the nonholonomic integrator, then several of the recently developed class of controllers that solve the unified tracking and regulation problem can be applied. A Lyapunov-based analysis is provided that illustrates a uniformly ultimately bounded tracking and regulation result.

REFERENCES

1. Brockett, R. W., "Asymptotic stability and feedback stabilization," In R. W. Brockett, R. S. Millman, and H. J. Sussmann (Eds) *Differential geometric control theory*, pp. 181–191 (1983).
2. Dixon, W. E., D. M. Dawson, E. Zergeroglu, and A. Behal, *Nonlinear Control of Mobile Robots, Lecture notes in Control and Information Sciences*, Springer-Verlag, London (2001).
3. Sira-Ramirez, H., C. Lopez-Uribe, and M. Velaso-Villa, "Linear observer-based active disturbance rejection control of the omnidirectional mobile robot," *Asian J. Control*, Vol. 15, No. 1, pp. 51–63 (2013).
4. Keighobadi, J. and M. B. Menhaj, "From nonlinear to fuzzy approaches in trajectory tracking control of wheeled mobile robots," *Asian J. Control*, Vol. 14, No. 4, pp. 960–973 (2012).
5. Wang, Z. and Y. Liu, "Global asymptotic stabilization control of a lake surface cleaning robot," In *Proc. of IEEE Int'l Conf. on Information and Automation*, Zhuhai/Macau, China, June 2009. pp. 271–276 (2009).
6. Morin, P. and C. Samson, "Control of nonholonomic mobile robots based on the transverse function approach," *IEEE Trans. Robot.*, Vol. 25, No. 5, pp. 1058–1073 (2009).
7. Dixon, W. E., D. M. Dawson, F. Zhang, and E. Zergeroglu, "Global exponential setpoint control of mobile robots," In *Proc. of the IEEE/ASME Int'l Conf. on Advanced Intelligent Mechatronics*, Atlanta, Georgia, pp. 683–688 (1999).
8. Morin, P. and C. Samson, "Practical stabilization of driftless systems on lie groups: the transverse function approach," *IEEE Trans. Autom. Control.*, Vol. 48, No. 9, pp. 1496–1508 (2003).
9. MacKunis, W., N. Gans, K. Kaiser, and W. E. Dixon, "Unified tracking and regulation visual servo control for wheeled mobile robots," In *Proc. IEEE Multi-conference on Systems and Control*, Singapore, pp. 88–93 (2007).
10. Smith, P. P., *Active Sensors for Local Planning in Mobile Robotics*. World Scientific Series in Robotics and Intelligent Systems, Vol. 26, World Scientific, Singapore (2001).
11. Tsakiris, D., P. Rives, and C. Samson, "Extending visual servoing techniques to nonholonomic mobile robots," In D. Kriegman (Ed.) *The confluence of vision and control, lecture notes in control and information systems*, Springer Verlag, Berlin, Germany, pp. 107–117 (1998).
12. Mariottini, G. L., G. Oriolo, and D. Prattichizzo, "Image-based visual servoing for nonholonomic mobile robots using epipolar geometry," *IEEE Trans. Robot.*, Vol. 23, No. 1, pp. 87–100 (2007).
13. Zhang, X., Y. Fang, and X. Liu, "Motion-estimation-based visual servoing of nonholonomic mobile robots," *IEEE Trans. Robot.*, Vol. 27, pp. 1167–1175 (2011).
14. Burschka, D. and G. Hager, "Vision-based control of mobile robots," In *Proc. of the IEEE Int'l Conf. on Robotics and Automation*, pp. 1707–1713 (2001).
15. Dixon, W. E., D. M. Dawson, E. Zergeroglu, and A. Behal, "Adaptive tracking control of a wheeled mobile robot via an uncalibrated camera system," *IEEE Trans. Syst. Man Cybern. Part B-Cybern.*, Vol. 31, No. 3, pp. 341–352 (2001).
16. Fang, Y., W. E. Dixon, D. M. Dawson, and P. Chawda, "Homography-based visual servoing of wheeled mobile robots," *IEEE Trans. Syst. Man Cybern. Part B-Cybern.*, Vol. 35, No. 5, pp. 1041–1050 (2005).
17. Samson, C., "Velocity and torque feedback control of a nonholonomic cart," In *Proc. Int'l Workshop in Adaptive and Nonlinear Control: Issues in Robotics*, Grenoble, France, pp. 125–151 (1990).
18. Chen, J., D. M. Dawson, W. E. Dixon, and A. Behal, "Adaptive homography-based visual servo tracking for a fixed camera configuration with a camera-in-hand extension," *IEEE Trans. Control Syst. Technol.*, Vol. 13, No. 5, pp. 814–825 (2005).
19. Chen, J., W. E. Dixon, D. M. Dawson, and M. McIntyre, "Homography-based visual servo tracking control of a wheeled mobile robot," *IEEE Trans. Robot.*, Vol. 22, No. 2, pp. 406–415 (2006).
20. Benhimane, S., E. Malis, P. Rives, and J. Azinheira, "Vision-based control for car platooning using homography decomposition," In Proc. of 2005 IEEE Int'l Conf. on Robotics and Automation, pp. 2161–2166 (2005).

© 2013 Chinese Automatic Control Society and Wiley Publishing Asia Pty Ltd

21. López-Nicolás, G., N. R. Gans, S. Bhattacharya, C. Sagüés, J. J. Guerrero, and S. Hutchinson, "Homography-based control scheme for mobile robots with nonholonomic and field-of-view constraints," *IEEE Trans. Systems Man Cybern. Part B-Cybern.*, Vol. 40, No. 4, pp. 1115–1127 (2010).
22. Bhattacharya, S., R. Murrieta-Cid, and S. Hutchinson, "Optimal paths for landmark-based navigation by differential-drive vehicles with field-of-view constraints," *IEEE Trans. Robot.*, Vol. 23, No. 1, pp. 47–59 (2007).
23. Dupree, K., N. Gans, W. MacKunis, and W. E. Dixon, "Euclidean calculation of feature points of a rotating satellite: A daisy chaining approach," *AIAA J. Guidance, Control, and Dynamics*, Vol. 31, No. 4, pp. 954–961 (2008).

William MacKunis received his Ph.D. degree in 2009 from the Department of Mechanical and Aerospace Engineering at the University of Florida (UF) as UF Alumni Fellow. After completing his doctoral studies, he was selected as National Research Council (NRC) Postdoctoral Research Associate at the Air Force Research Laboratory Munitions Directorate at Eglin Air Force Base, where he worked in the Guidance and Navigation Division. In 2010, Dr MacKunis joined the Physical Sciences Department at Embry-Riddle Aeronautical University in Daytona Beach, FL, where he is currently Assistant Professor of Engineering Physics. Dr MacKunis' research focus is in Lyapunov-based control techniques for nonlinear mechanical systems with uncertain or ill-defined dynamic models. He is the co-author of over 40 refereed journal and conference papers and the monograph RISE-Based Robust and Adaptive Control of Nonlinear Systems, and his research has been recognized by NASA, NSF, and NRC.

Nicholas Gans earned his B.S. degree in electrical engineering from Case Western Reserve University, Cleveland OH, in 1999. He received the M.S. degree in electrical and computer engineering and his Ph.D. in systems and entrepreneurial engineering from the University of Illinois at Urbana-Champaign in December 2005. He held postdoctoral positions with the Mechanical and Aerospace Engineering Department at the University of Florida and with the National Research Council through the US Air Force Research Laboratory. Since 2009, he has been Assistant Professor in the Department of Electrical Engineering at the University of Texas at Dallas. His research interests include nonlinear and adaptive control, with focus on vision-based control and estimation, robotics and autonomous vehicles.

Anup Parikh received his Bachelor of Science degree in both Mechanical and Aerospace Engineering from the University of Florida. As an undergraduate, he designed and fabricated a MEMS hot film shear stress sensor as an alternative to more expensive floating-element sensors. As a graduate researcher in the Nonlinear Controls and Robotics group, his interests include vision based estimation and control of UAV quadrotors and other aerospace systems. He is currently pursuing a PhD at the University of Florida under the advisement of Dr. Warren Dixon.

Prof. Warren Dixon received his Ph.D. in 2000 from the Department of Electrical and Computer Engineering from Clemson University. After completing his doctoral studies he was selected as Eugene P. Wigner Fellow at Oak Ridge National Laboratory (ORNL). In 2004, Dr. Dixon joined the University of Florida in the Mechanical and Aerospace Engineering Department, where he currently is the Charles Taylor Faculty Fellow and holds a University of Florida Research Foundation Professorship. Dr. Dixon's main research interest has been the development and application of Lyapunov-based control techniques for uncertain nonlinear systems. He has published 3 books, an edited collection, 9 chapters, and over 250 refereed journal and conference papers. His work has been recognized by the 2012–2013 University of Florida College of Engineering Doctoral Dissertation Mentoring Award, 2011 American Society of Mechanical Engineers (ASME) Dynamics Systems and Control Division Outstanding Young Investigator Award, 2009 American Automatic Control Council (AACC) O. Hugo Schuck Award, 2006 IEEE Robotics and Automation Society (RAS) Early Academic Career Award, an NSF CAREER Award (2006–2011), 2004 DOE Outstanding Mentor Award, and the 2001 ORNL Early Career Award for Engineering Achievement. He is an IEEE Control Systems Society (CSS) Distinguished Lecturer. He currently serves as a member of the U.S. Air Force Science Advisory Board and as the Director of Operations for the Executive Committee of the IEEE CSS Board of Governors. He is currently or formerly Associate Editor for ASME Journal of Journal of Dynamic Systems, Measurement and Control, Automatica, IEEE Transactions on Systems Man and Cybernetics: Part B Cybernetics, and the International Journal of Robust and Nonlinear Control.

© 2013 Chinese Automatic Control Society and Wiley Publishing Asia Pty Ltd